Tyre/road interaction noise-Numerical noise prediction of a patterned tyre on a rough road surface

Tyre / Road Interaction Noise - Numerical noise prediction of a patterned tyre on a rough road surface

D.J. O'Boy *, A.P.Dowling

Department of Engineering, University of Cambridge

Abstract

The noise which results from the interaction of pneumatic tyres with a rough road surface is a significant contributor to an increasing local environmental problem. Above a steady forward vehicle speed of 40 km/hr this is the dominant noise source of a modern car in good working condition, and is a significant contributor to the overall radiated noise during acceleration.

In order to determine the noise produced by a patterned tyre rolling on a rough road surface, the vibration characteristics of the tyre must be known. A method has been presented by O'Boy and Dowling [1] which provides these vibration characteristics for a tyre belt comprised of multiple viscoelastic layers, each layer having a different thickness and material properties. In this paper, we use this model of the tyre belt to determine the parameters of an equivalent simple bending plate model which can be adapted to yield the response of a tyre which includes sidewalls.

A method is then described which uses this response to determine the acceleration of the tyre surface as it rolls over a rough road. These accelerations are then used to predict the far field radiated noise for a patterned tyre on two rough road surfaces. Comparisons with experimental data are provided at each stage.

Key words: Tyre, noise, vibration, viscoelastic multilayer structure, far-field pressure

1 Introduction

The noise generated by the interaction of vehicle tyres with a road surface is a significant contributor to a growing local environmental problem [2]. For modern passenger cars in good condition travelling at steady speed, the tyre / road interaction noise is the dominant noise source above 40 km/hr [3] (this also applies for certain trucks meeting EU vehicle regulations and more generally at a slightly higher speed). During acceleration this source is a significant contributor to the overall noise generated and above approximately 50 km/hr is the dominant noise source.

In order to determine the noise produced by a patterned tyre rolling on a rough road surface, the vibration characteristics of the tyre must be known. A tyre is composed of sidewalls, connected by a tyre belt which is covered with a thick layer of tread rubber. Although the vibration of the sidewalls also generate sound, this paper will present results for the sound of the tyre belt only. The tyre belt is a complicated multilayer structure, made with different materials of differing thicknesses. Furthermore the tread pattern may be a complicated arrangement of blocks in the circumferential and axial directions.

* Corresponding author. Department of Engineering, University of Cambridge, Trumpington Street, Cambridge, CB2 1PZ
Email address: djo31@cam.ac.uk (D.J. O'Boy).
URL: http://www.eng.cam.ac.uk/~djo31 (D.J. O'Boy).

There are many ways of obtaining the response of a tyre when excited either radially or tangentially. Finite element methods are best suited to lower frequency ranges or for use at single frequencies, due to the computational demands [4], however they allow anisotropic material properties. For tyre noise, interest is in the response in the 0.3 - 2 kHz frequency range and then the common approach is to make simplifications and assumptions to restrict the complexity of the model to shell and bending plate models [5][6][7]. However, there is then the issue of determining the parameters in the simplified models used to describe the belt vibration. These are usually found empirically through comparison with experimental data. Not surprisingly, these produce good agreement for comparisons between the experimental tyre and the model but this does not provide a predictive capability for different tyres. Investigations into new belt materials and / or different material thicknesses would potentially require a new experimental tyre belt to be constructed and tested each time, at potential cost to the tyre manufacturer. This does not therefore provide a way of minimising the radiated sound through a theoretical optimisation. However, the advantages of this method are that the experiments can be performed on the actual tyre and model parameters obtained without needing to know exact details of the construction of the tyre. Indeed, due to manufacturing tolerances and changes to the dimensions of each layer during manufacture, the actual tyre is tested, without needing to take into account irregularities in each layer. The main disadvantages to this method (other than cost) are that the number of tyres which can be tested are limited by the number which can feasibly be produced. This method also does not allow any detailed physical insight into the stress and displacement in each layer.

This paper presents a method which uses the results presented in O'Boy and

Dowling [1] of a viscoelastic tyre belt model to obtain the parameters for a simplified bending plate model using only data on material properties that would be available in the design process before a tyre is manufactured. The response of a bending plate is determined and compared to this existing comprehensive numerical model of a tyre belt which provides the displacement and velocity response of a multilayer cylindrical viscoelastic tyre belt when excited either radially or tangentially by a force. In section 3 the parameters for the equivalent bending plate are then optimised to minimise the error between the response of the bending plate and the multilayer viscoelastic model.

A bending plate with these parameters is then used in an existing model of a finite width tyre (see Blakemore [16] or Graf [17]), which takes into account the effect of the sidewalls and air pressure and the response of this tyre is determined. In section 4 as a validation exercise, the response of the tyre to point harmonic excitation is determined. These results are compared to experimental measurements taken on a real tyre corresponding to the design data used to define the viscoelastic model.

A description is provided in section 5 of a method which can be used to obtain the acceleration of a tyre surface when rolling at speed across a rough road surface. In section 6 these accelerations are used to obtain predictions of the sound pressure around the tyre, taking into account the amplification from the horn effect, which is compared with the measured sound field. This sound can be defined as the structure-borne noise generated by the vibration of the tyre surface.

2 Description of the multilayer cylindrical tyre belt model

In order to be able to predict the sound from a rolling tyre on a rough road surface, the vibration characteristics of the tyre belt, located between the tyre sidewalls and excluding the tread layer must be known. Specifically, the response of the surface is required when excited radially. Since the aim of this paper is to show a method to predict the rolling tyre / road interaction noise without requiring access to experimental measurements, only design data used at the tyre manufacturing stage is used.

The tyre belt response is provided using the multilayer cylindrical viscoelastic model from O'Boy and Dowling [1], which takes into account the material properties and the thickness of each layer. An air cavity is included between a fixed wheel hub and the layers of material of the tyre belt, as shown in Fig. 1.

In O'Boy and Dowling [1], a relationship between the three components of displacement u_r, u_θ, u_y and traction $\sigma_{rr}, \sigma_{r\theta}, \sigma_{ry}$ on the outer surface of the tyre belt and those on the inner surface of the tyre belt were determined, using the product of material matrices for each layer of the belt (which contain the information on the material properties, thickness and radius);

$$\begin{pmatrix} \tilde{\boldsymbol{\sigma}} \\ \\ \tilde{\mathbf{u}} \end{pmatrix}_{r_{N+1}} = \prod_{j=1}^{N} \mathbf{X}_j \begin{pmatrix} \tilde{\boldsymbol{\sigma}} \\ \\ \tilde{\mathbf{u}} \end{pmatrix}_{r_1} . \tag{1}$$

The notation is similar to [1], where $\tilde{\mathbf{u}}$ and $\tilde{\boldsymbol{\sigma}}$ denote the Fourier transform of the displacement and stress variables. The radius of the belt is given by r, the time represented by t and the spatial coordinates, θ and y the angle around

the circumference and axial distance respectively. In the Fourier domain these become frequency ω, angular order n and axial wavenumber k_y.

$$\tilde{u}(r,\omega,n,k_y) = \int_{-\infty}^{\infty}\int_{-\infty}^{\infty}\int_{-\pi}^{\pi} u(r,\theta,y,t)\, e^{-\mathrm{i}n\theta}\, e^{-\mathrm{i}k_y y}\, e^{-\mathrm{i}\omega t}\, \mathrm{d}\theta\, \mathrm{d}y\, \mathrm{d}t, \tag{2}$$

$$u(r,t,\theta,y) = \frac{1}{(2\pi)^3}\int_{-\infty}^{\infty}\int_{-\infty}^{\infty}\sum_{n=-\infty}^{\infty} \tilde{u}(r,n,k_y,\omega)\, e^{\mathrm{i}n\theta} e^{\mathrm{i}k_y y} e^{\mathrm{i}\omega t}\mathrm{d}k_y\, \mathrm{d}\omega. \tag{3}$$

Through application of six boundary conditions, including a representation of an air cavity on the inner surface of the belt and a force applied to the outer surface, the Fourier transform of displacement or velocity of the outer surface of the tyre belt may be determined as a function of frequency, angular order and axial wavenumber. The most useful vibration data for use in a noise prediction programme for a vehicle moving at steady speed is the radial displacement of the belt when a radial force is applied. This is described by the transfer function $\tilde{u}_r/\tilde{\sigma}_{rr}(r,\omega,n,k_y)$. Also of use is the point mobility, which refers to the radial velocity resulting from a radial force input, $\tilde{v}_r/\tilde{\sigma}_{rr}(r,\omega,n,k_y)$, where $\tilde{v}_r = \mathrm{i}\omega\tilde{u}_r$. The formula for the inverse Fourier transform, Eq. (3) may be applied to these responses to obtain the displacements and velocities due to a specified force as functions of the spatial coordinates.

The results of the multi-layer model will be compared to those of a tensioned bending plate and with the same applied force an error minimisation routine is used to adjust the plate parameters until the optimum plate description is found, one which minimises the difference between the tyre belt and the plate response.

3 Flat bending plate approximation of a tyre belt

A bending plate with normal displacement w (in the z direction), applied load per unit area p, mass per unit area M, in-plane tension T, and thickness h has an equation of motion which may be written [8],

$$T\nabla^2 w(x,y,t) - D\nabla^4 w(x,y,t) + p + \eta_p\sqrt{DM}\frac{\partial}{\partial t}\nabla^2 w = M\frac{\partial^2 w(x,y,t)}{\partial t^2}, \quad (4)$$

where x, y define the plane of the plate, the term ∇ is the vector operator $(\partial/\partial x_1, \partial/\partial x_2)$ and the bending stiffness $D = Eh^3/(12(1-\nu^2))$, where E and ν are Young's modulus and Poisson's ratio respectively.

In the frequency domain, plate damping is including by allowing the bending stiffness and / or the tension to become complex [9]. An additional damping term is included which is proportional to the Laplacian of the plate velocity, as introduced by Crighton [10], where the constant of proportionality is written as $\eta_p\sqrt{DM}$ and η_p is a small positive constant.

In the derivation of the equation for a bending plate it is assumed that the deformation in the plate is small in comparison to the thickness. During pure bending, the forces required to bend the plate are significantly less than the internal extension and compression forces. Prior to the application of the bending moment the plate has a neutral axis located at half the thickness and lines may be drawn through the material linking the top and bottom surfaces at normal angles. Once the moment is applied these lines are still at right angles to the top surface (in compression), the neutral surface and bottom surface (in extension) as shear deformations are assumed negligible.

This derivation assumes that any rotary inertia is negligible in relation to the

magnitude of the translational motion. The effects of both shear deformation and rotary inertia were included by Mindlin [11] using a Timoshenko shear coefficient κ [12] and the Lamé constant μ, which yield a far more accurate response. The accuracy of the equations prior to the inclusion of these terms is studied by Cremer, Heckl and Ungar [13] who calculated that the correction terms would make less than a ten percent difference if the flexural wavelength was greater than six times the thickness of the plate. The range of validity is therefore $\lambda > 6h$, which expressed as a wavenumber is $k < 2\pi/6h$. The tyre belt, excluding the outer tread has a thickness of 10.54 mm and therefore has a maximum wavenumber of around 100 rad/m. If the layer of tread rubber is included, it is clear that the inclusion of the rotary inertia and shear deformation terms are necessary, which modifies Eq. (4)[8],

$$T\nabla^2 w(x,y,t) + \left(\nabla^2 - \frac{\rho}{\kappa^2\mu}\frac{\partial^2}{\partial t^2}\right)\left(\frac{\rho h^3}{12}\frac{\partial^2}{\partial t^2} - D\nabla^2\right) w(x,y,t) + k_s w(x,y,t) - \eta_p\sqrt{DM}\frac{\partial}{\partial t}\nabla^2 w + \left(1 - \frac{D\nabla^2}{\kappa^2\mu h} + \frac{\rho h^2}{12\kappa^2\mu}\frac{\partial^2}{\partial t^2}\right) p(x,y,t) = M\frac{\partial^2 w(x,y,t)}{\partial t^2}. \quad (5)$$

To represent a tyre, it is also assumed that Eq. (4) is modified so that the plate is resting on equivalent distributed springs of stiffness k_s (as described in Graff [8]) and dampers as used in the viscoelastic model [1] (these distributed springs are a simplified representation of the sidewalls), with an equivalent impedance on its upper surface as that due to the air cavity force in the cylindrical viscoelastic model shown in Fig. 2. The forward Fourier transform is performed over time t and axial direction y on Eq. (4) and the plate is taken to be periodic in the x direction, with a length equivalent to the circumference of the tyre, transforming x to n/R, where R is the radius of the tyre. The

transformed deformation is then given by

$$\tilde{w}(\omega, n, k_y) = \frac{\tilde{p}[I_0 k_y^2 + I_1]}{\Psi_1 k_y^4 + [\Psi_2 + I_2]k_y^2 + [\Psi_3 + I_3]},$$

where the terms associated with the simple bending plate Ψ and those correction terms associated with the shear deformation and rotary inertia are given by,

$$\Psi_1 = D, \tag{6}$$
$$\Psi_2 = 2Dn^2/R^2 + T + \mathrm{i}\omega\eta_p\sqrt{DM}, \tag{7}$$
$$\Psi_3 = Dn^4/R^4 + Tn^2/R^2 + \mathrm{i}\omega\eta_p\sqrt{DM}n^2/R^2 + k_s - M\omega^2, \tag{8}$$
$$I_0 = D/(\kappa^2\mu h), \tag{9}$$
$$I_1 = 1 + Dn^2/(\kappa^2\mu h R^2) - \omega^2\rho h^2/(12\kappa^2\mu), \tag{10}$$
$$I_2 = -\omega^2(\rho h^3/12 + D\rho/(\kappa^2\mu)), \tag{11}$$
$$I_3 = -\omega^2(\rho h^3/12 + D\rho/(\kappa^2\mu))n^2/R^2 + \omega^4\rho^2 h^3/(12\kappa^2\mu). \tag{12}$$

These equations relate to a single plate undergoing pure bending. For one isotropic layer of material, the neutral surface is at a distance of half the thickness and the bending stiffness is given from Eq. (4). Since the tyre belt is made of multiple layers of material, it is necessary to determine a way to obtain the equivalent bending stiffness for a multilayer plate. An analytical method is available for three layers of material [14] although this makes assumptions to the relative stiffness of the different layers, therefore a numerical method has been developed which is applicable for any number of layers and material properties.

4 Numerical determination of plate parameters for a tyre belt

A numerical method is described in this section which determines the parameters for the equivalent plate model which best matches the response to

forcing of the viscoelastic cylindrical structure, with specified number of layers of different materials. These equivalent plate parameters are obtained by comparing the response of a bending plate with the results obtained from the viscoelastic model [1] and iteratively adjusting the plate parameters until any differences between the two responses are minimised. In this manner it is then possible to determine the parameters for a plate which yields the equivalent response as the tyre belt.

Since the displacement response of the bending plate to forcing is $W = \tilde{w}(\omega, k, n)/\tilde{p}$ and the response of the viscoelastic tyre belt model is given by $U = \tilde{u}_r(r, \omega, k, n)/\tilde{\sigma}_{rr}$, then an appropriate error function $E(\omega, k, n)$ is $U - W$, a function of the frequency, axial wavenumber and equivalent angular wavenumber and bending plate parameters. The problem is then one of finding the plate parameters which minimise this error, over a wide frequency and wavenumber range. The method used is the Downhill Simplex method introduced by Nelder and Mead [15], which requires an initial guess for the parameters and then steps towards a local minima as shown in Fig. 3. To determine the global minima curve, the initial starting point must be inside the global minima curve (i.e. between points P_1 and P_2 which locates the minimum B). Many minimisation methods could have been chosen, however, the Nelder and Mead routine does not require any derivative information and is relatively quick and numerically stable. The error between the viscoelastic belt and the plate must be minimised over a range of frequencies, angular orders and axial wavenumbers. In order to achieve this, consider the example in Fig. 4, where the initial plate and viscoelastic belt responses are plotted for a specific value of frequency and axial wavenumber against angular order, n. The initial plate parameters have ensured that the starting point for the simplex locates the

flexural vibration peak of the plate in the dominant flexural vibration peak of the belt. Either side of this peak, there are markers, n_L and n_H. The ideal equivalent plate parameters should match the amplitude and as far as possible the shape of the dominant flexural vibration peak, in addition to the mean amplitude at low angular orders.

To accomplish this, the measure of the error between the two responses is defined in two parts with the weighting between the two given by α (this weighting is determined empirically to ensure the minimisation method is stable and follows the global minima).

$$E(\omega, k, n) = \alpha \sum_{n=0}^{n_L} \frac{(U(n) - W(n))^2}{U(n)^2} + (1 - \alpha) \sum_{n=n_L}^{n_H} \frac{(U(n) - W(n))^2}{U(n)^2}. \quad (13)$$

The former component minimises the error at low values of angular order while the latter matches the amplitude of the peak. The summation is completed over angular order and axial wavenumber to provide a set of parameters which yield the best equivalent bending plate to the viscoelastic tyre belt, for a specific frequency. The optimisation routine fixes the mass per unit area of the tyre, the dimensions (width and radius), air pressure and spring stiffness, then adjusts the bending stiffness, damping rates and tensions iteratively.

4.1 Bending plate parameters for a tyre belt

The multivariable optimisation method is now used to determine the plate parameters which give the equivalent response as the viscoelastic tyre belt model [1]. These parameters are determined for the case of a tyre belt and also a tyre covered with a thick layer of smooth tread rubber on the outside surface.

The plate parameters are determined for a frequency range between 200 Hz and 2 kHz, over a range of angular orders and axial mode numbers. For a plate with a mass per unit area of 14 kg/m^2, the range of values of the bending stiffness is shown in Fig. 5(a) with the magnitude of the complex and Crighton damping coefficients against frequency in Figs. 5(b) and (c) respectively. The bending stiffness rises to a maximum at 600 Hz before decreasing for increasing frequency. The magnitude of the Crighton damping decreases at higher frequencies where the complex damping term increases. Since the plate does not exactly model the amplitude response of the cylindrical structure at low angular orders, a large value of damping is therefore required to provide the equivalent amplitude response. Furthermore, since the bending plate may only support one wave type, the comparison at low angular orders and axial wavenumbers will always be a best-fit approximation as the viscoelastic model has an amplitude response comprised of thickness modes, shear modes (if excited by the boundary conditions) and flexural wave modes. At higher frequencies, where the excitation wavelength is short, the individual material properties of each layer become more important, leading to further differences.

The optimisation process provides equal weighting to every parameter, which is also a factor in the variations with frequency. A further improvement may require that individual parameters are assumed to be more important than others, alternatively, different optimisation routines could be tested.

The variation in the parameters with frequency is also partly due to the variation in the Timoshenko shear coefficient κ which is required with changing frequency. Taking the average values of the established parameters with equal weighting given to each frequency yields the equivalent bending stiffness of 7.6 Nm, complex damping factor 0.11 and a magnitude of the Crighton damp-

ing factor of 0.12. The magnitude of the in-plane tension is 70 kN/m. The equivalent plate response for the tyre belt may now be direction compared to the response provided by the viscoelastic tyre belt model, Fig. 6(a). The response of the plate is shown in 6(b) for the axial mode $m = 0$ for a frequency range 0-2 kHz (the axial wavenumber $k_y = m\pi/w$ where m is the axial mode and w the width of the tyre). It may be seen that although the amplitude is overestimated at frequencies below f=100 Hz and slightly underestimated at frequencies above f=1800 Hz, the broad shape of the curve is matched and the average amplitude correctly determined. The tyre belt excludes the thick layer of tread rubber into which the tread pattern is formed. The response of the tyre belt with this layer has been previously determined using the viscoelastic tyre model and parameters determined for a bending plate which give an equivalent response. For a mass per unit area of 21.8 kg/m^2 (calculated using engineering drawings and data on each layer of the tyre belt), the equivalent bending stiffness is 13.6 Nm, complex damping 0.21 and Crighton damping 0.22. The variation of bending stiffness with frequency is shown in Fig. 7(a) which is reasonably stable apart from the very low and very high frequency ranges. This could result from trying to match a curve to a very low amplitude signal or, one which is very close to the origin of the angular order axis. The variations of the magnitude of the complex damping and Crighton damping with frequency are shown in Figs. 7(b) and (c) respectively, where the Crighton damping dominates at low frequencies and the complex at higher frequencies. Since the outer layer is now a relatively soft rubber layer, there is a much stronger vibration mode associated with the compression of the rubber, which will influence the overall equivalent parameters. As with the previous case, the variations in the parameters with frequency are also due to comparing a plane geometry with a cylindrical geometry and variations in the

shear coefficient at low and high frequencies. In addition, the high damping present in the tread rubber leads to a lower amplitude vibration for higher angular orders and axial modes.

The average plate parameters are used to deduce the equivalent plate response for a tyre belt with a thick layer of tread rubber. This is compared to the response of the viscoelastic tyre belt model which also includes the tread in Fig. 8(a) and (b). Although the amplitude responses of the two are slightly different, the resonant frequencies are located correctly for both the lower and upper range of angular modes.

4.2 Finite bending plate model of the tyre

The tyre belt models described in previous sections have all assumed periodicity in the axial direction (the sidewalls being infinitely stiff line springs at the nodal points), so that the axial wavenumber is $k_y = m\pi/w$, where m is the mode number and w the width of the tyre. A finite bending plate model is available which provides a more accurate representation of the sidewalls, from Blakemore [16], and determines the Green's function of a finite width tyre (this Green's function, denoted $G_{\beta\alpha}(t)$ is the displacement of the tyre surface in the radial direction, at a tread block β, when a radial stress is applied as an impulse function at tread block location α).

The tyre is modelled as a flat orthotropic plate undergoing bending which is periodic in the x direction (representing the circumferential direction). Sidewalls are included using line springs located at either axial edge, which cannot support moments from the belt. The internal tyre pressure is represented as a

distributed force proportional to the displacement of the surface and tensions in the belt in both the circumferential T_x and axial T_y directions are included. The model of the finite width tyre utilises parameters provided in the previous sections, for example the bending stiffness, damping, mass and belt tensions. The width of the tyre is assumed to be w=0.18 m, although it is recognised that the sidewalls are curved rather than vertically straight.

The bending stiffness for the case of a tyre with and without a thick layer of tread rubber has been determined and it is noted that the two figures are different. The individual tread blocks on a patterned tyre are formed by cutting grooves in this outer rubber layer, yielding an overall bending stiffness somewhere between the two extremes. To determine the bending stiffness of a patterned tyre belt (with 280 tread blocks arranged in five rows), we calculate the proportion of the tyre surface area covered by the tread blocks. This is used as a weighting function between the bending stiffness for a tyre belt with and without a thick layer of tread rubber. This simplification yields a bending stiffness for the patterned tyre of 12 Nm.

It has been assumed until now that each layer in the tyre is isotropic in the circumferential and axial directions. However, the breaker layers contain steel cords laid at an angle of $\pm 21^{\circ}$ to the circumferential direction, which make the overall tyre belt orthotropic, with a different value of bending stiffness in the circumferential and axial directions. This change is estimated to yield a bending stiffness in the axial direction of 8 Nm. The stiffness of the springs representing the sidewalls are estimated from calculations provided in Graf [17] (where the stiffness is estimated proportional to the internal air pressure) and from experiments performed on a static tyre (showing load deflection data) to be 4.24 MN/m^2, with an associated damping coefficient of 0.2 magnitude.

The distribution of springs on the inside surface of the tyre representing the air pressure are estimated to have a stiffness of 0.2 MN/m^3 which only affect those modes which involve compression of the volume of air inside the tyre.

The predicted Green's function for the patterned tyre is calculated and compared with dynamic tyre measurements made by Taylor [18] using an unloaded test tyre with regular tread pattern, supplied by Dunlop Tyres. The tread pattern on the tyre consisted of five rows of tread blocks across the width and fifty six blocks in each row around the circumference, the arrangement shown in Fig. 9. Each tread block measured 3.0 cm by 2.6 cm by 8 mm thick and for the purposes of the experiment, are numbered from 1 to 56 around the circumference (the distance between tread blocks is 3.6 cm). The first tread block in each of the first three rows (labelled the outer, middle and centre tread rows) were excited using an electromagnetic shaker driven with a broadband white noise signal in both radial, tangential and lateral directions. A force transducer was positioned between the shaker and the tread block surface and the components of acceleration at subsequent tread blocks in the row obtained. The transfer function giving the radial acceleration of block α to radial force excitation at block β is then obtained by dividing the acceleration by the force (this is termed the accelerance). The comparisons are only shown for frequencies up to 1 kHz as the signal to noise ratio in the experimental measurements decreases with increasing frequency. The strict validation therefore only applies in this frequency range, although the numerical model will be utilised for higher frequencies and sound predictions.

The accelerance of a tread block when radially excited in the centre tread block row is shown in Fig 10. The plate cannot reproduce the very low frequency behaviour which is the difference between a plane and cylindrical structure.

There is a fairly good amplitude match up to around 600 Hz between the finite width tyre model and the experimental measurements although the phase between the two moves so that the location of the peaks and troughs no longer match at all frequencies.

The transfer functions relating the radial surface velocity to the radial forcing function is shown for the subsequent four tread blocks on the centre row of the tyre in Figs. 11(a), (b), (c) and (d) respectively. Although the amplitude is broadly correct, there is some error in the location of the resonances. It can be seen that differences between the predictions and measurements are greatest further away from the forcing location and for frequencies over 800 Hz. However, the high damping present in the materials means that the overall amplitude of displacement will be lower for measurement positions away from the contact patch, especially at the higher forcing frequencies, when the forcing position remains constant.

The predicted point mobility response of the tyre, defined as the radial velocity response of the tyre surface, to an applied radial forcing is shown in Fig. 12 for θ=0^o against frequency and axial position across the tyre width. The excitation force is applied at different tread block rows in the axial direction and the amplitude of the surface velocity shown as contours, where a light colour indicates a high response. The case where the tyre is forced in the centre row is indicated in Fig. 12(a), which shows that the majority of the energy is located below a frequency of 2 kHz and a significant proportion below 1 kHz. The case where the tyre is forced in the middle row of tread blocks, Fig. 12(b) shows that the high damping present in the materials attenuates vibrations on the far side of the tyre, except for frequencies less than 500 Hz.

The case where the outer row is forced displays high velocities at the edge of the tyre, where the resistive force from the sidewalls dominates the resistance from the bending stiffness of the tyre. It is also the case that when forcing closer to the edge of the tyre, that only half of the material area is available to dissipate energy with, compared to the case of forcing in the centre tread.

Bolton [19] has also produced similar decompositions from experiments on a Firestone P215/70R14 tyre, excited radially with a force transducer while held fixed on a tyre balancer. When examining plots of normalised radial velocity, two waveforms may be identified, which he concludes are from a small number of slowly propagating flexural modes (with speeds between 60-80 m/s), dependent on the inflation pressure and a faster set of modes, from the extension of the tyre belt (with speeds $\approx$ 170 m/s). The bending plate model used for the predictions in this section could only support flexural waves and is incompressible, so only the former wave type can be predicted. In the time domain, Fig. 13 these predicted waves from the numerical model may be seen to travel from the impact point around the circumference of the tyre, reflecting back and forth from the sidewalls, with a speed of between 50-70 m/s (for illustrative purposes, the figure shows the bending plate curved into a cylindrical tyre shape).

5 Prediction of the rolling response of the tyre surface

Now that the stationary tyre response is known, a method may be developed to obtain the displacement of any point on the tyre surface while rolling. The tyre vibration resulting from a rolling contact with a road surface requires a relationship between the force on a single tread block f_α and the displacements

of the tyre belt u_α^{belt} and the tread block u_α^{tread} to be known. These may be defined using the undeformed radii of the tyre r and the radii of the belt and tread blocks r_α^{belt} and r_α^{tread} respectively, as $u_\alpha^{\text{belt}} = r - r_\alpha^{\text{belt}}$ and $u_\alpha^{\text{tread}} = r - r_\alpha^{\text{tread}}$ as shown in Fig. 14. As the tyre rotates, the tread blocks which are located at the leading edge will impact the surface and become compressed as they enter the contact patch, expanding as they leave it. The displacement of the tread blocks and the surface of the tyre belt as functions of time, as they move over a rough road surface can be obtained using the method developed by Graham [20] and Kropp [7][21], where the displacement of the tyre belt at a block β at time t to an applied force at block α at time t' is a function of a convolution.

$$u_\beta^{\text{belt}}(t) = \int_{-\infty}^{t} G_{\beta\alpha}(t - t') \; f_\alpha(t') \, \mathrm{d}t'. \tag{14}$$

Then a summation over N tread blocks may be employed to yield the overall displacement.

$$u_\beta^{\text{belt}}(t) = \sum_{\alpha=1}^{N} \int_{-\infty}^{t} G_{\beta\alpha}(t - \tau) \; f_\alpha(\tau) \, \mathrm{d}\tau. \tag{15}$$

Each tread block in the contact patch is compressed, with the tread block rubber having a stiffness k_{blk}, an uncompressed height of H_{blk}, with zero mass. The force is therefore given by $f_\alpha = k_{blk}(H_{blk} + u_\alpha^{\text{tread}} - u_\alpha^{\text{belt}}) \, H_v$, where the term H_v is a Heaviside function which allows the force to be set to zero when the tread block is outside of the contact patch, using the road surface height given by u_α^{road} (when the block is in contact with the road surface, then $u_\alpha^{\text{road}} = u_\alpha^{\text{tread}}$). It is defined as $H_v = 1$ for $H_{blk} + u_\alpha^{\text{road}} - u_\alpha^{\text{belt}} > 0$ and $H_v = 0$ for $H_{blk} + u_\alpha^{\text{road}} - u_\alpha^{\text{belt}} < 0$. The road surface height is averaged over the area of one tread block in order to approximate the deformation which occurs in the tread rubber.

These equations are discretised with a time step of Δt and a trapezoidal

method used to integrate the convolution of the Green's function with the force from the road surface over the time τ. If the discrete time series is $\tau = J\Delta t$, where J is an integer number of timesteps, then integrating over one time segment yields,

$$\int_{[J-1]\Delta t}^{J\Delta t} G_{\beta\alpha}(t - J\Delta t)\ f_\alpha(J\Delta t)\ \mathrm{d}\tau = \frac{\Delta t}{2}\left\{G_{\beta\alpha}(t - [J-1]\Delta t)\ f_\alpha([J-1]\Delta t) + G_{\beta\alpha}(t - J\Delta t)\ f_\alpha(J\Delta t)\right\}. \quad (16)$$

Completing the discrete sum from $j{=}-\infty$ to J and rearranging gives the discrete equation used to determine the displacement of the tyre surface as it rolls over a rough surface, where $G_{\beta\alpha}(0) = 0$ if $\beta \neq \alpha$.

$$u_\beta^{belt}(t) - \frac{\Delta t}{2} G_{\beta\alpha}(0)\ f_\alpha(t) = \sum_{\alpha=1}^{N} \sum_{j=-\infty}^{J-1} \Delta t\ G_{\beta\alpha}(t - j\Delta t)\ f_\alpha(j\Delta t). \quad (17)$$

The simulation commences with the tyre out of contact with the road surface, $f_\alpha(0) = 0$ and the displacement of the tread blocks can then be found using Eq. (17). The simulation time is then incremented by Δt, the wheel is lowered slightly, the wheel and road are rotated and translated respectively according to the prescribed vehicle speed and the new forces on the tread blocks are determined using the new road heights and tread block compressions.

As this iterative process repeats, the wheel is slowly lowered onto the road surface, increasing the force on the wheel hub until the required mean load is reached. This iterative process steps forward in time and gives the displacement of the tyre surface for each row of tread blocks as it rolls over the road surface.

Three incompressible road surfaces are considered for investigation into the tyre surface vibration as it rolls at speed; a fully smooth road surface, an

ISO-10844 specification (International Organisation for Standardisation) and one comprised of hot rolled asphalt (HRA). The ISO-10844 (also known by the British Standard, BS-10844) specifies a relatively smooth standard road surface texture used to produce consistent levels of road noise and is not considered representative of road surfaces used in the United Kingdom. By contrast, the hot rolled asphalt surface is used for a high percentage of the UK road network and is defined in BS-594 with a minimum required texture height of 1.5 mm.

One dimensional height profiles of these surfaces were measured by S. Kollamthodi of TRL Limited with a laser profilometer taking longitudinal measurements every 0.2 mm with a vertical resolution of 0.01 mm [20]. These one dimensional road profiles were subsequently converted into a representative two dimensional height by Graham [20] (see also Graf [17]).

5.1 Vibration resulting from a patterned tyre rolling on a smooth road surface

The surface vibration of a rolling tyre is now predicted for the case of a patterned tyre with two hundred and eighty regularly spaced tread blocks across five rows, rolling on a smooth road surface at a forward speed of 80 km/hr, using 1500 numerical steps per revolution of the tyre (the time for one revolution, $T_{\text{rev}} = 90$ ms). The number of computational steps was iteratively chosen to be the minimum required to capture the high frequency vibration. Experimental measurements were also performed on a tyre equivalent to that used to define the computational model. This tyre was fixed to a rotating drum and equipped with an accelerometer embedded in the tread, to measure the acceleration of the tyre surface as the tread blocks entered and left the contact

patch. The force on a tread block was also measured, for the centre row of tread blocks. Ideally, the tyre is designed to spread an even load over all of the tread blocks in the contact patch during coasting conditions. Although the shape of the actual contact patch would be more of a ellipse, with a greater load concentrated at the centre, the same experimental data has been used to compare the predicted load on the middle and outer rows of tread blocks. A static load of 420 kg was applied to the experimental tyre at the axle. The force transducer is designed to capture the force profile distributed over a whole tread block, rather than the smaller scale and more difficult to measure frictional loading across the tread block.

The method used to obtain the predicted rolling response of the tyre requires that at time $t = 0$ s, the tyre is out of contact with the road surface, to provide known initial conditions over the whole tyre surface. In order to approximately replicate the total axle load, the tyre was slowly lowered by a vertical distance of 15 mm (determined through empirical numerical calculations) over a period of a quarter of a tyre revolution. A further one revolution was performed to allow any transient vibrations to sufficiently attenuate before measurements were taken. A comparison of the total load on the outer, middle and centre rows of tread blocks are shown in Figs. 15 (a), (b) and (c) respectively assuming an axial curvature of 1.6 /m of the tyre surface. The total load on the tread rows is shown in Fig. 15(d). It may be seen that the total load on the centre row of tread blocks is slightly higher than the middle row of tread blocks, with the load decreasing slightly for the outer row. The total load has an average which is approximately 4.1 kN, which agrees well with the required experimental conditions. For a real tyre, the load on the tread blocks across the tyre width would be expected to be approximately equal for the centreline,

so that the wear rate is equivalent. The variation in load seen in the finite width model is most likely a result of using a constant bending stiffness in the axial direction, whereas a real tyre will have a variation towards the sidewalls through a change in thickness of the materials and manufacturing technique, yielding a different curvature.

The force on the surface of one tread block as it enters and leaves the contact patch, for the outer, middle and centre rows of tread blocks is shown in Figs. 16(a), (b) and (c) respectively. The predicted force oscillates far more than the experimental data would indicate, possibly due to neglecting the unsprung mass and damping of the tread blocks. The area under the force profiles for the outer, middle and centre rows are 11 N, 14 N and 15 N respectively, which may be compared to the area under the experimental force profile (12 N). One possible explanation for this difference is that the predicted contact patch is slightly shorter due to the rise in temperature of the tyre surface in the experimental measurements. However, the force profile is reasonable and we may assume that any predictions for the vibration on a rough road surface will be a reasonable reflection of actual tyre vibration data.

A comparison between the computed block acceleration and the experimentally measured equivalent is shown in Figs. 17(a)-(d) for a tyre rotating at 80 km/hr. It can be seen that the damping present in the tyre belt causes the amplitude of the waves travelling out from the contact patch to attenuate rapidly.

As the blocks rotate with the tyre, they experience a centripetal acceleration, which is indicated as zero on the graphs. As the block enters the contact patch, it experiences a rapid deceleration, which for the experiment is slightly less

than -2000 m/s^2, but for the model is slightly above -2000 m/s^2. The difference is most likely due to neglecting the block mass. The predicted accelerations are also slightly higher, for all tread block rows, which could be due to the shorter contact patch length mentioned earlier. The waves at the leading edge of the contact patch have a different frequency content than the waves at the trailing edge, which for the experimental case is measured to be 912 Hz (leading) and 483 Hz (trailing) with an average of 697 Hz. Depending on the radius of the compressed tyre as it travels along the road at 22.2 m/s (80 km/hr), the impact frequency f_i, of the tread blocks is estimated to be in the range 600-690 Hz, which occurs at the leading edge of the contact patch. Using fixed ground coordinates, the tread blocks are equivalent to a wave travelling in the same direction as the tyre rotation with a speed of 22.2 m/s. These impacts cause a bending wave to propagate from the contact patch around the tyre circumference, whose speed has been estimated to be in the range 50-70 m/s. These two waves interfere, causing a Doppler shift in the frequency at the leading edge and in the contact patch. The shifted frequency forward of the tread block impacts is given by $f_1 = f_i(1 + u/c_B)$, where u is the forward vehicle speed and the frequency moving towards the trailing edge is shifted by $f_2 = f_i(1 - u/c_B)$ (c_B is the relevant bending wave speed at that given frequency). At the leading edge of the contact patch, where the tread blocks first begin to impact the surface, only the impact frequency and the associated harmonics are found.

6 Far field sound prediction

The far field sound pressure is predicted in two stages, the first being to find the pressure distribution due to a number of sound sources on the tyre surface in free air, without any solid tyre geometry, as shown in Fig. 18(a). This is combined with a transfer function which provides the amplification between the sound field with no tyre and with the tyre geometry shown in Fig. 18(b) (termed the horn amplification), where the circumferential position around the tyre is defined by $x_{\text{belt}} = R\theta$.

Initially the pressure field due to a source on a control surface around the tyre is determined, using a Green's function $G(\mathbf{y}, t|\mathbf{x}, \tau)$ which provides the response at a position given by the three-dimensional coordinate vector $\mathbf{y}$ at time t to a pulse released at a position $\mathbf{x}$ at time τ. This function satisfies the wave equation with a speed of sound c. We also define a pressure disturbance in a sound field $p'(\mathbf{x}, t)$ which also satisfies the wave equation. It can be shown that the far field pressure can be expressed as a function of a integral over the control surface, see for example Rienstra [22], where we specify that normal to the control surface the Green's function is zero, $\partial G(\mathbf{y}|\mathbf{x})/\partial n = 0$. The far field pressure is then $p'(\mathbf{y}, \omega) = \int_S G(\mathbf{y}|\mathbf{x})(\partial p'/\partial n)\,\mathrm{d}S$, where S defines the path of the surface.

Using the conservation of momentum, the pressure normal to the tyre surface may be expressed as a function of the tyre surface velocity $\partial p'/\partial n = -\rho_0 \mathrm{i}\omega v(S)$, which is related to the surface acceleration by noting that $-\mathrm{i}\omega v(S) = a(S)$, as previously utilised with success by Eberhardt [23] and Graf [17].

It remains to find the Green's function $G(\mathbf{y}|\mathbf{x})$ that satisfies $\partial G/\partial n = 0$ on

the plane surface and on the tyre. Without the tyre, the Green's function for a source at $\mathbf{x}$ in three-dimensional free space bounded by a rigid plane is $G(\mathbf{y}|\mathbf{x}) = e^{(-\mathrm{i}k|\mathbf{y}-\mathbf{x}|)}/(2\pi|\mathbf{y}-\mathbf{x}|)$, where $k = \omega/c$, c is the speed of sound in air and $\mathbf{x}$ is near the plane surface. The geometry between the tyre and the road surface creates a shape similar to a gramophone horn, which has the effect of amplifying any sound sources present. This amplification has been numerically characterised by Graf [17] for a range of frequencies and positions around the tyre surface using a Boundary Element Method (BEM) code with a tyre shaped mesh in contact with a half plane (with an impedance of 10 GNs/m^3) and is defined as the amplification between the pressure found with the tyre geometry p_{tyre} and without the tyre geometry p_{free},

$$G_{\mathrm{horn}}(\mathbf{x},\omega) = p_{\mathrm{tyre}}(\mathbf{x},\omega)/p_{\mathrm{free}}(\mathbf{x},\omega). \tag{18}$$

Using this transfer function for the horn amplification, the far field pressure can be written, using a discrete sum over the tyre surface, where the term ΔA is the elemental surface area.

$$p'(\mathbf{y},\omega) = \frac{\rho_0}{2\pi}\sum \frac{a(\mathbf{x},\omega)}{|\mathbf{y}-\mathbf{x}|}e^{-\mathrm{i}k|\mathbf{y}-\mathbf{x}|}G_{\mathrm{horn}}(\mathbf{x},\omega)\Delta A. \tag{19}$$

Comparisons are made between predictions and equivalent experimental measurements carried out by the Transport and Research Laboratory (TRL). A TRL tyre testing vehicle (a modified Suzuki Vitara) was equipped with seven microphones (only five will be detailed as the remaining two are used for reference measurements) around the rear off-side wheel, mounted on a thin metal frame shown in Fig. 19. The rear tyre, a patterned test tyre equivalent to the one used in the computations, was loaded to 420 kg and noise measurements

carried out at vehicle speeds of 70, 80 and 90 km/hr as the vehicle travelled over the two rough road surfaces. Due to wind contamination, it is considered that the results for frequencies lower than 250 Hz are considered unreliable for comparison.

6.1 Far field sound predictions compared with experimental measurements

The far field pressure signal is determined computationally for each of the five microphone positions on the two rough surfaces under consideration and the power spectral density (PSD) taken, defined as the measure of the distribution of energy in a signal, displayed in the frequency domain. The power spectral densities for both of the experimental measurements and the computational predictions are shown with the energy in equivalent frequency bands, in decibels (dB) with an A-weighting applied.

The power spectral density signal is shown in Fig. 20 for the five microphone positions of interest, relating to a patterned tyre rolling over an ISO-10844 specification road surface at 80 km/hr. The predictions provide a fairly good representation of the broad band sound, for almost all microphone positions. The method over-predicts the energy at the discrete frequencies of the tread block impact and its harmonics, especially at positions towards the rear of the tyre.

The predictions of the power spectral density against experimental measurements for a patterned tyre rolling on an ISO specification surface at a speed of 90 km/hr are shown in Fig. 21. The predictions are reasonably accurate for microphone positions forward of the tyre with greater errors appearing for

microphone locations towards the rear of the tyre. It may be seen that the ISO specification surface tends to excite the frequencies associated with the tread block pattern, with little broadband excitation. Therefore, if the tyre design were to be optimised for minimal radiated sound using this surface, only the tread pattern would tend to be changed.

The power spectral density predictions for a patterned tyre rolling on a hot rolled asphalt surface at 80 km/hr are shown in Fig. 22. As with the predictions on an ISO surface, there is good agreement with the experimental measurements for microphone positions forward of the tyre, in terms of locating the position and amplitude of the tread block impact frequency and the broadband excitation. The predictions are less accurate for microphone positions towards the rear of the tyre, which could indicate that the stick-slip vibration of the tread blocks exiting the contact patch could be more important. This trend can also be seen in the results for the tyre rolling on the ISO-10844 road surface. The comparisons for the higher speed of 90 km/hr are shown in Fig. 23. The hot rolled asphalt surface tends to yield a greater level of broad band excitation in the tyre structure. The characteristics of the sound are very different from the measurements on the ISO surface and it is likely that any optimisation of the tyre structure for noise reduction would lead to changes in the belt properties in addition to the tread block distribution pattern.

7 Conclusions

In order to determine the noise produced by a patterned tyre rolling on a rough road surface, the vibration characteristics of the tyre must be known. A method has been presented in O'Boy and Dowling [1] which provides these vi-

bration characteristics for a tyre belt comprised of multiple viscoelastic layers with different thickness and material properties. In this paper, a methodology was successfully demonstrated to determine the parameters of a simple bending plate model which would yield the equivalent response as this tyre belt, without requiring experimental measurements. This equivalent bending plate model of a tyre belt may be modified so that it can represent the sidewalls of a tyre and therefore produce predictions of the radial response of a tyre. These predictions have been compared to experimental measurements with good agreement, although differences have been noted and we conclude that these are primarily due to representing the tyre structure as an incompressible plane structure.

This finite width tyre model has been used to produce transfer functions relating the radial acceleration of the tyre surface to a radial forcing excitation, which is applied at one of five different rows of tread blocks. The comparisons between the experimental results and the predictions show that the results are most accurate close to the forcing location, with errors increasing for locations further away as the response is attenuated.

A method has then been described which uses this transfer function, together with the force from the contact patch at any given time, to determine the acceleration of the tyre surface as the tyre rolls at speed over a smooth or rough road. Predictions of the force on a single tread block are given, with good agreement with experimental measurements, in addition to comparisons of the acceleration of a tread block as it enters and leaves the contact patch. The change in the wave-speed due to the Doppler shift is successfully predicted, as is the attenuation rate of the amplitude of the acceleration.

Finally a method is provided which allows the far field sound pressure to be determined using the knowledge of the surface acceleration of the tyre. Predictions of the radiated sound pressure from a patterned tyre rolling over two rough road surfaces, a hot rolled asphalt conforming to British Standard BS-594 and an ISO-10844 specification road surface at two different forward vehicle speeds of 80 and 90 km/hr.

It has been shown that the ISO specification surface has such a smooth texture that it excites little broad band noise and accentuates the sound resulting from the main tread pattern impact frequencies. Any noise reduction work which utilises this road surface will therefore only lead to changes which optimise the tread block impact frequencies. By contrast, the hot rolled asphalt, which is more representative of common rough road surfaces, excites both broad band noise and also the tread block impact frequencies and any noise reduction work undertaken on this surface will therefore lead to changes in the tyre belt structure in addition to the tread pattern.

The results of the noise predictions show that both of the above trends are correctly identified in common with the experimental results. For microphone positions forward of the tyre, the comparisons show good agreement, as this is where the radial vibration of the tyre produces the dominant noise. For microphone positions which are to the rear of the tyre, the comparisons show greater errors, which is most likely due to neglecting the vibrations caused by stick-slip action as the tread block vibrate tangentially upon exiting the contact patch.

Acknowledgements

My appreciation to the Engineering and Physical Sciences Research Council (EPSRC) for funding this work, as well as Goodyear Dunlop tyres, LandRover and TRL for providing facilities, experimental results and industrial information on tyre dynamics and design. My thanks also to Dr Graf for the use of the horn amplification data, and Dr Graham for the time-stepping program.

References

[1] D. O'Boy, A. Dowling, Tyre / road interaction noise: A 3d viscoelastic multilayer model of a tyre belt., submitted for consideration to the Journal of Sound and Vibration. Copy of paper available via the Internet at http://www2.eng.cam.ac.uk/~djo31/JSVpaper/DanOBoy1.pdf.

[2] Future noise policy, COM(96)540, European Commission, Green Paper (1996).

[3] U. Sandberg, Tyre/road noise - myths and realities (plenary paper), in: Proceedings of the International Congress and Exhibition on Noise Control Engineering, the Netherlands, 2001.

[4] M. Brinkmeier, U. Nackenhorst, von Estorff O., S. Petersen, Physically based modelling of tire-rolling-noise by a finite element approach, in: Proceedings of Internoise, 2004.

[5] R. Keltie, Analytical model of the truck tire vibration sound mechanism, Journal of the Acoustical Society of America 71 (2) (1982) 359–367.

[6] Y.-J. Kim, S. Bolton, Modeling tire tread-band vibration, in: Proceedings of Internoise, 2001.

[7] W. Kropp, A mathematical model of tyre noise generation, Heavy Vehicle Systems, International Journal of Vehicle Design 6 (1-4) (1999) 310–329.

[8] K. Graff, Wave Motion in Elastic Solids, Clarendon Press, Oxford, 1975.

[9] D. Crighton, A. Dowling, J. Ffowcs Williams, M. Heckl, F. Leppington, Modern methods in Analytical Acoustics, Springer-Verlag, 1992.

[10] D. Crighton, Wave motion and vibration induced by turbulent flow, Ph.D. thesis, Imperial College London (1968).

[11] R. Mindlin, Influence of rotary inertia and shear on flexural motions of isotropic, elastic plates, Journal of Applied Mechanics 18 (1951) 31–38.

[12] S. Timoshenko, On the correction for shear of the differential equation for transverse vibrations of prismatic bars, Phil.Mag. 6 (41) (1921) 744.

[13] M. Heckl, L. Cremer, E. Ungar, Structure Borne Sound, 2nd Edition, Springer-Verlag, 1988.

[14] D. Ross, E. Kerwin, E. Ungar, Damping of plate flexural vibrations by means of viscoelastic laminae, Structural Damping 3 (1959) 44–87.

[15] J. Nelder, R. Mead, A simplex method for function minimisation, The Computer Journal 7 (1965) 308–313.

[16] M. Blakemore, Calculation of the Green's function for a tyre belt, in Understanding Road Generated Noise from Tyres (URGENT), IST-054 EPSRC GR/M09056/01 and GR/M11431/01, Tech. rep., Department of Engineering, University of Cambridge, UK (March 2002).

[17] R. Graf, Tyre-road interaction noise, Ph.D. thesis, Department of Engineering, University of Cambridge (2002).

[18] N. Taylor, Tyre dynamic measurements, in Understanding Road Generated Noise from Tyres (URGENT), IST-054 EPSRC GR/M09056/01 and

GR/M11431/01, Tech. rep., Department of Engineering, University of Cambridge, UK (March 2002).

[19] J. Bolton, H. Song, Y. Kim, Y. Kang, The wave number decomposition approach to the analysis of tire vibration, in: Proceedings of NOISE-CON, 1998.

[20] A. Dowling, W. Graham, R. Graf, Understanding Road Generated Noise from Tyres (URGENT), IST-054 EPSRC GR/M09056/01 and GR/M11431/01, Tech. rep., Department of Engineering, University of Cambridge (March 2002).

[21] W. Kropp, K. Larsson, F. Wullens, P. Andersson, Tyre/road noise generation - modelling and understanding, in: Proceedings of the Institute of Acoustics, 2004.

[22] S. Rienstra, A. Hirschberg, An introduction to acoustics (extended and revised version of IWDE 92-06), Tech. rep., Eindhoven: Technische Universiteit Eindhoven (2001).

[23] A. Eberhart, Investigation of the truck tire vibration sound mechanism, in: International Tire Noise Conference, 1979.

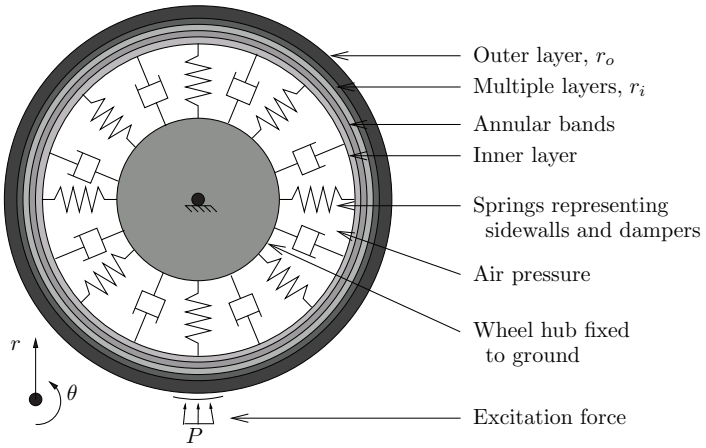

Fig. 1. Complete viscoelastic cylindrical model of the tyre belt.

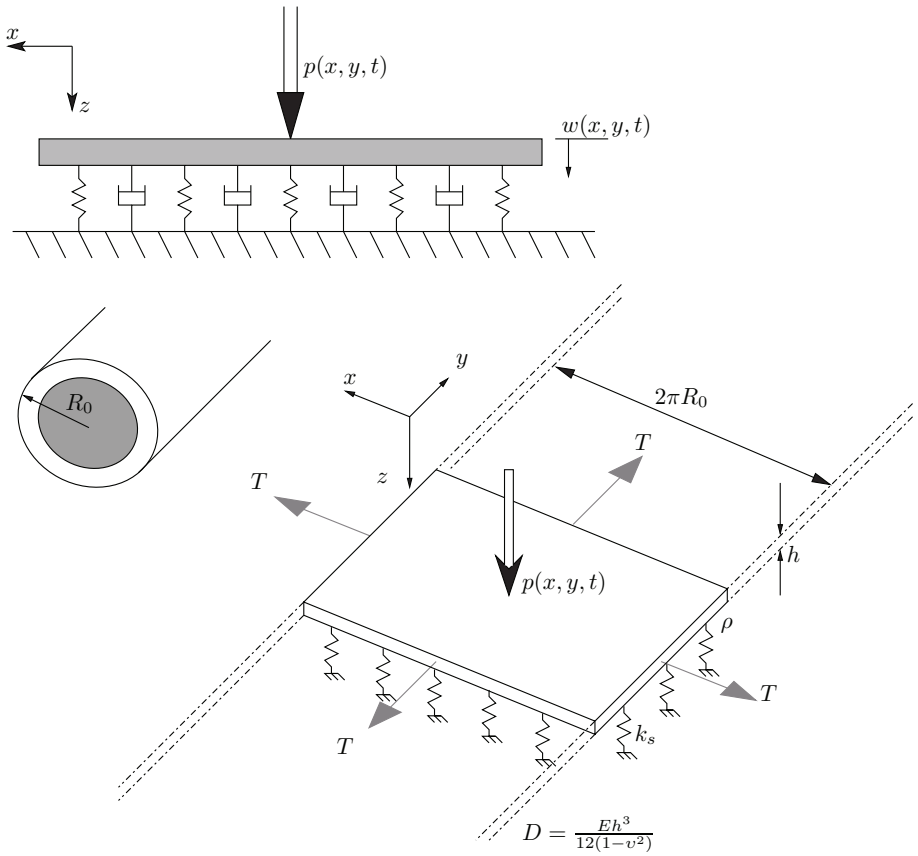

Fig. 2. Diagram of a thin bending plate with infinite width and in-plane tension, used for comparison to the viscoelastic multilayer tyre belt.

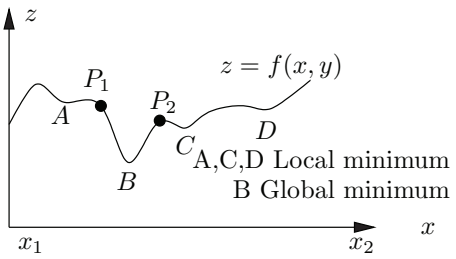

Fig. 3. Local and global minimum of function $z = f(x, y)$ with initial starting point of error minimisation routine.

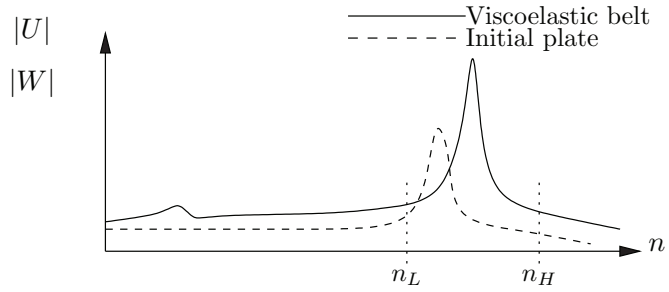

Fig. 4. Initial plate response before error minimisation. The response of the viscoelastic belt is illustrated, with a dominant flexural peak. The equivalent plate response should match the shape and amplitude of this peak, in addition to the low angular order amplitude.

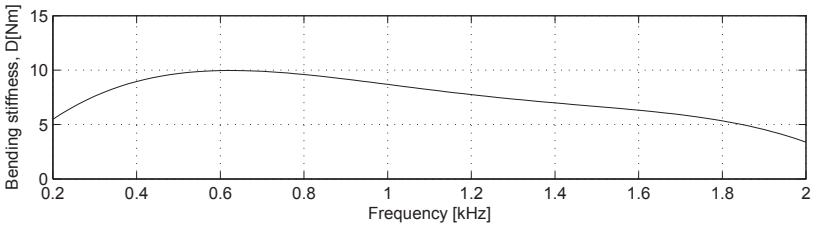

(a)

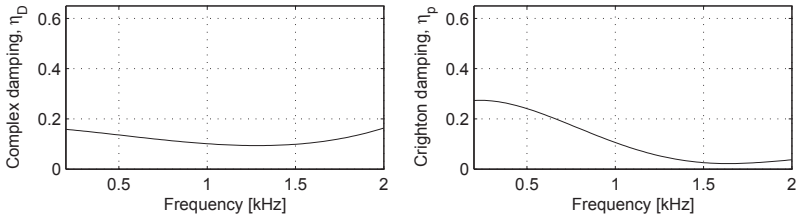

(b) (c)

Fig. 5. Equivalent bending plate parameters for a viscoelastic tyre belt. (a) Equivalent bending stiffness against frequency [Nm]; (b) Magnitude of complex damping; (c) Magnitude of the Crighton damping term.

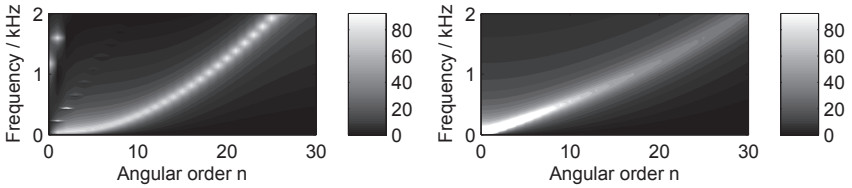

(a) (b)

Fig. 6. Comparison of the velocity response of the viscoelastic tyre belt model without a thick layer of tread rubber, $|\tilde{v}_r/\tilde{\sigma}_{rr}|$ $[10^{-9}(\mathrm{m}^3/\mathrm{N})]$ with the equivalent plate $|\tilde{\tilde{w}}/\tilde{p}|$ $[10^{-9}(\mathrm{m}^3/\mathrm{N})]$ for the $m = 0$ axial mode of vibration. (a) Viscoelastic tyre belt; (b) Equivalent plate.

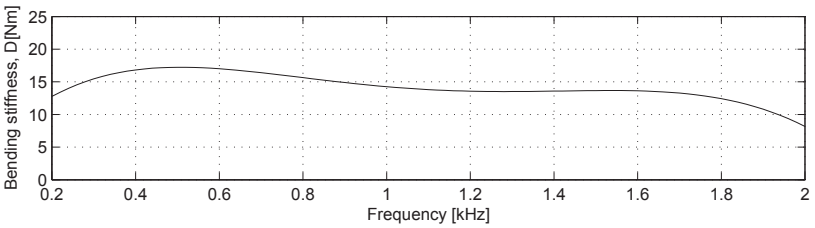

(a)

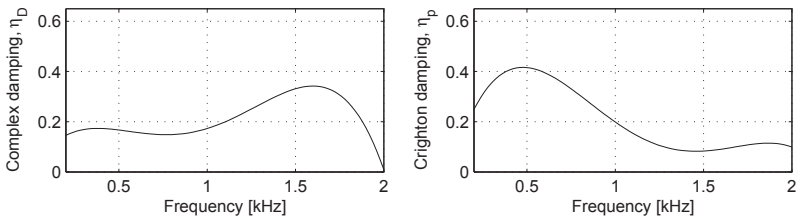

(b) (c)

Fig. 7. Equivalent plate parameters for a viscoelastic tyre belt including a thick layer of tread rubber. (a) Equivalent bending stiffness against frequency [Nm]; (b) Magnitude of the complex damping; (c) Magnitude of Crighton damping.

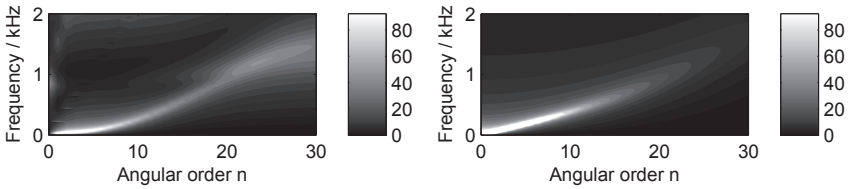

Fig. 8. Comparison of the velocity response of the viscoelastic tyre belt model with a thick layer of tread rubber, $|\tilde{v}_r/\tilde{\sigma}_{rr}|$ $[10^{-9}(\mathrm{m}^3/\mathrm{N})]$ with the equivalent plate $|\tilde{\tilde{w}}/\tilde{p}|$ $[10^{-9}(\mathrm{m}^3/\mathrm{N})]$, for the $m = 0$ axial mode. (a) Viscoelastic tyre belt and tread; (b) Equivalent plate.

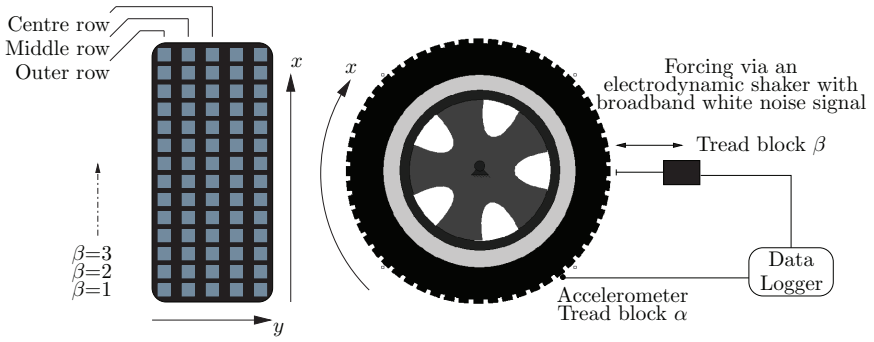

Fig. 9. Obtaining the transfer function between two tread blocks of a tyre. One block is forced at block β and the acceleration response obtained at block α.

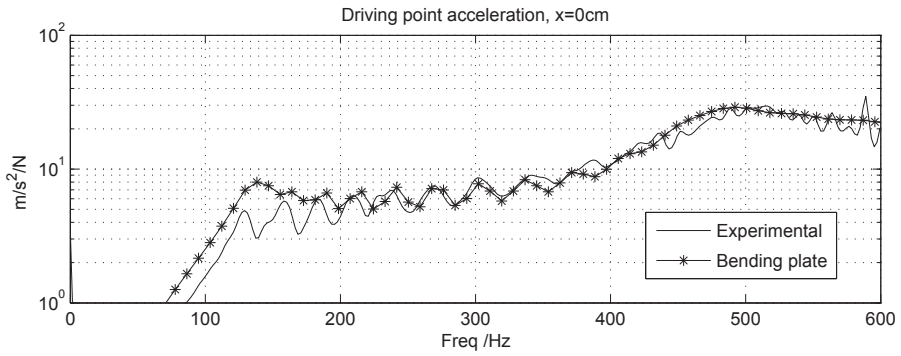

Fig. 10. Point accelerance showing radial acceleration at a tread block to radial harmonic forcing at the same tread block for the centre row of tread blocks.

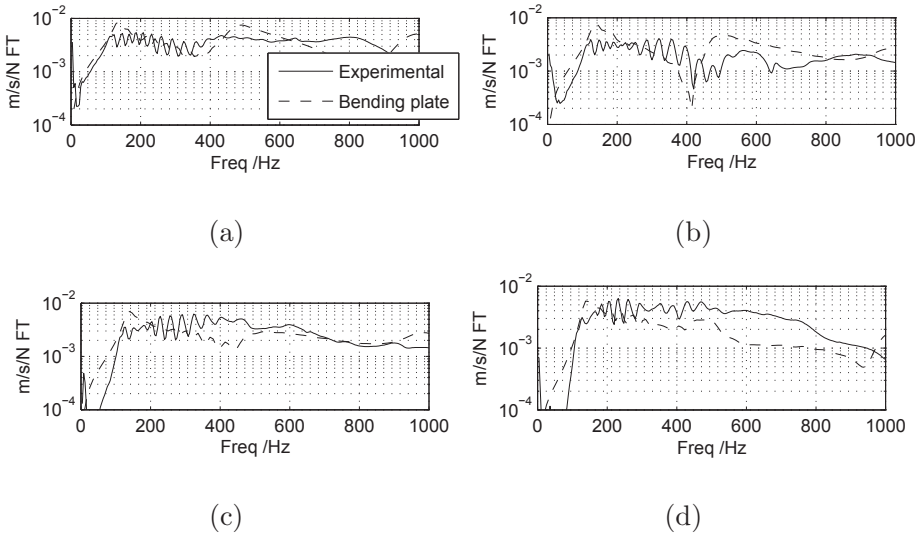

Fig. 11. Transfer functions showing radial velocity at tread block α to radial harmonic forcing at tread block β for the centre row of tread blocks. (a) Block α =2; (b) Block α =3; (c) Block α =4; (d) Block α =5.

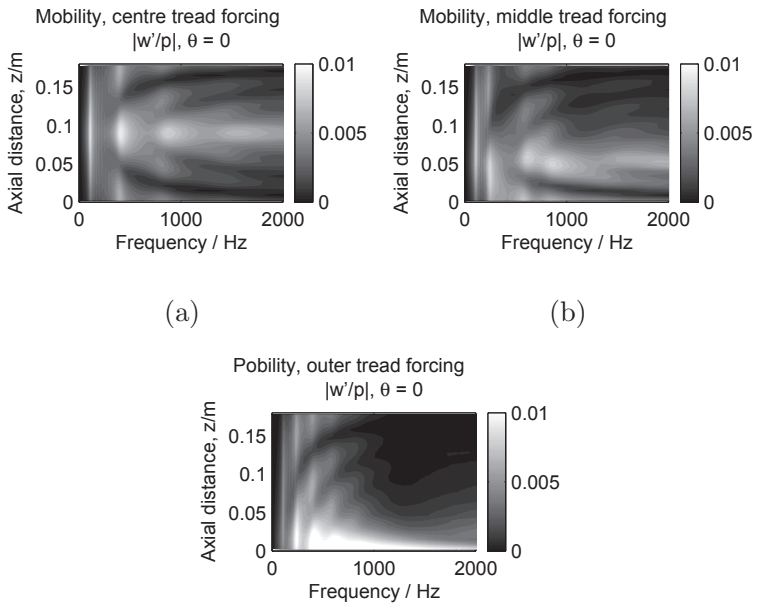

(a) (b)

(c)

Fig. 12. Numerical mobility predictions, defined as the radial velocity response of the tyre surface, for an applied radial forcing. The mobility for the case where different rows of tread blocks are forced, as a function of frequency and axial position are shown for the circumferential position $\theta = 0^o$. (a) Mobility where the centre row of tread blocks is excited; (b) The middle row of tread blocks is excited; (c) The outer row of tread blocks is excited.

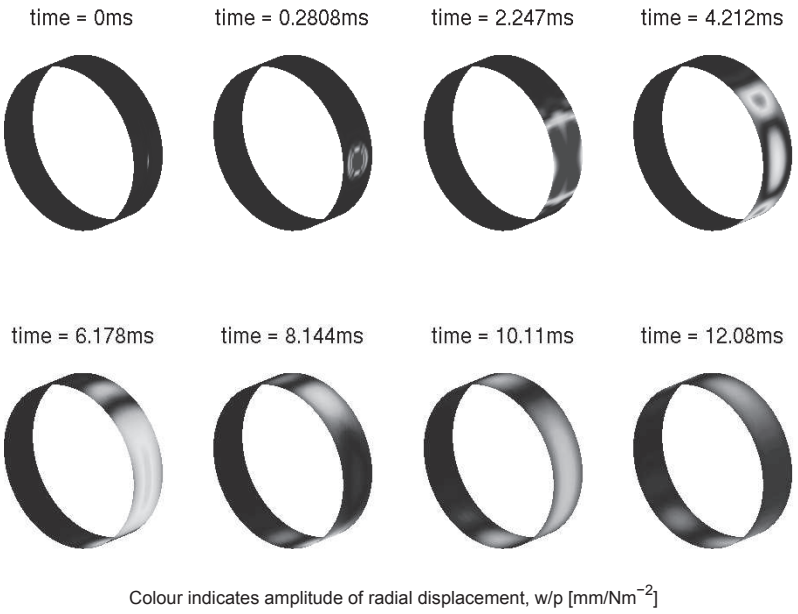

Fig. 13. Impulse response of the finite width tyre in the time domain, $|w/p|[10^{-3}(\mathrm{m}^3/\mathrm{N})]$, forcing a tread block in the centre row. Incremental time steps are shown with the colour gradient indicating the amplitude of the response (the predictions for the bending plate have been superimposed onto a cylindrical shape).

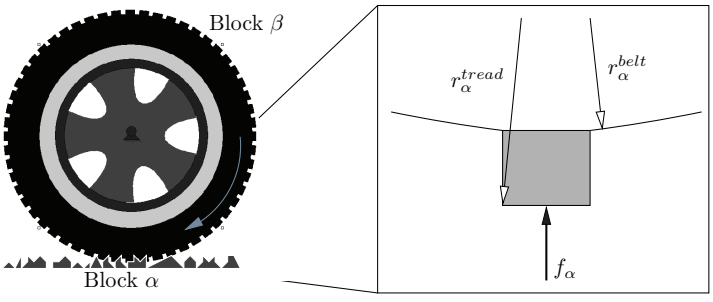

Fig. 14. The notation used to define the displacements of the tyre belt and tread blocks as they roll over a rough road surface.

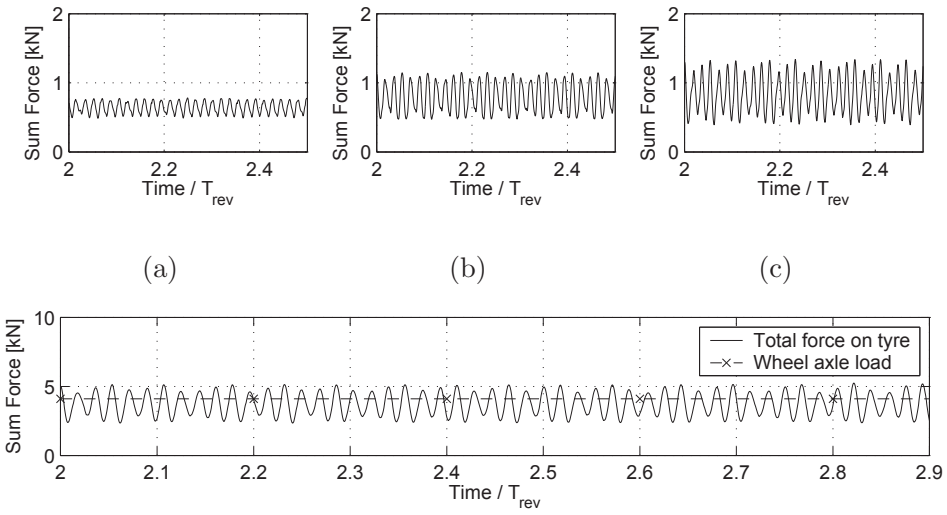

Fig. 15. Sum of the force on different rows of tread blocks for a tyre rolling on a smooth road surface with a forward speed of 80 km/hr. (a) Sum of the force on the outer row of tread blocks; (b) Sum of the force on the middle row; (c) Sum of the force on the centre row of tread blocks; (d) Total predicted force on the tyre against static axle load applied to the tyre used for experimental measurements.

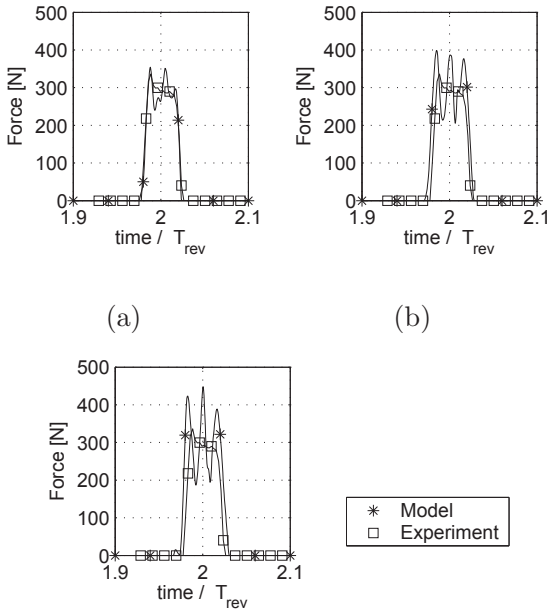

Fig. 16. Amplitude of the force on a tread block as it enters the contact patch compared with experimental data. The road surface is smooth with a patterned tyre rolling at 80 km/hr. (a) Force profile for a tread block fixed to the outer row of tread blocks; (b) Force profile for a block on the middle row; (c) Force profile for a block on the centre row.

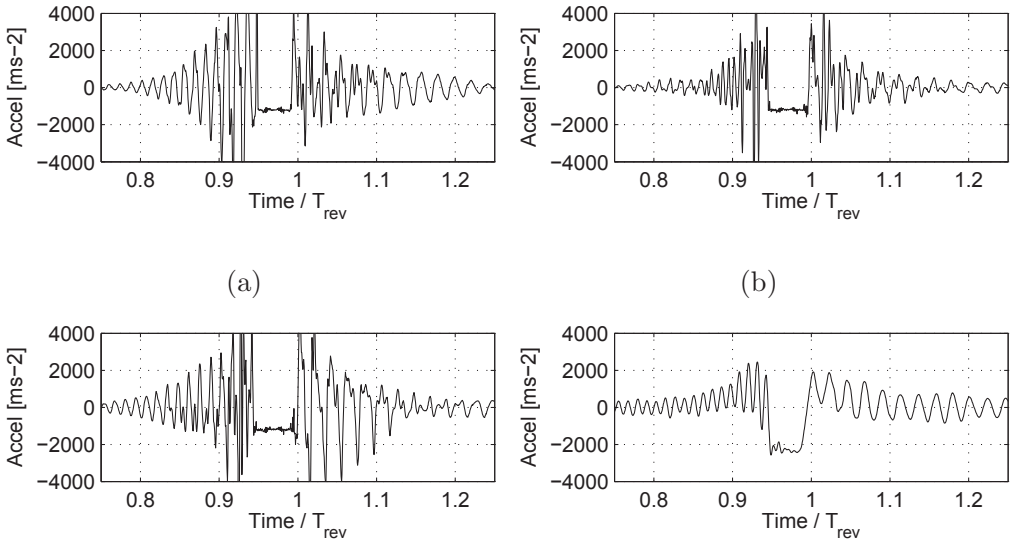

Fig. 17. Comparison of the acceleration of a tread block on each tread row, entering and leaving the contact patch, with experimental data. The road surface is smooth with a patterned tyre rolling at 80 km/hr. (a) Acceleration of a block from the outer row of tread blocks; (b) Acceleration of a block from the middle row of tread blocks; (c) Acceleration of a block from the centre row of tread blocks; (d) Experimentally measured tread block acceleration.

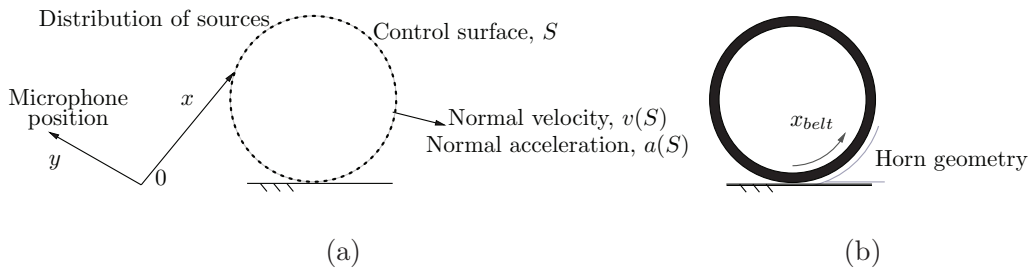

Fig. 18. The far field sound is predicted by integrating individual sound sources over the surface of the tyre. The amplification due to the solid geometric shape of the tyre is then introduced via a transfer function. (a) Distribution of sound sources on surface of tyre; (b) Tyre geometry which leads to the horn amplification, where the circumferential position around the tyre is defined by x_{belt}. As x_{belt} increases, a diverging space is present, similar to a gramophone horn, which amplifies sound sources present.

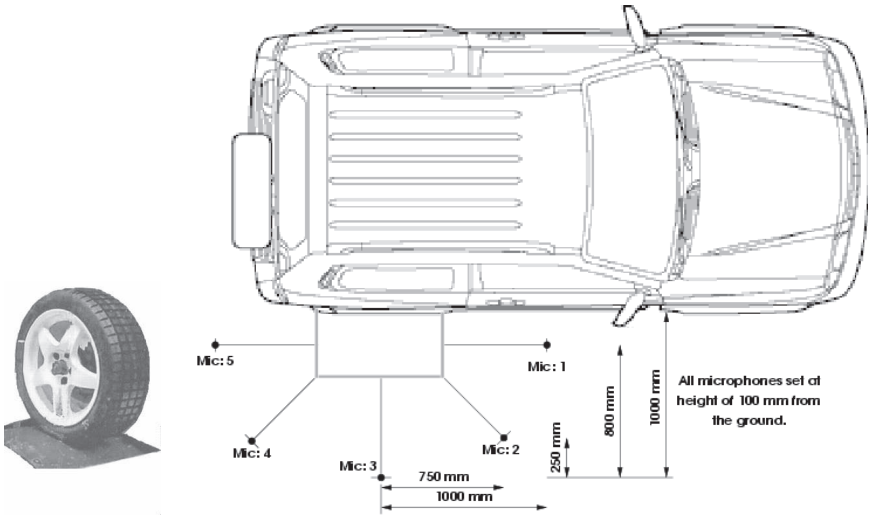

Fig. 19. Photograph of the patterned test tyre and microphone positions as applied to the test vehicle, a Suzuki Vitara.

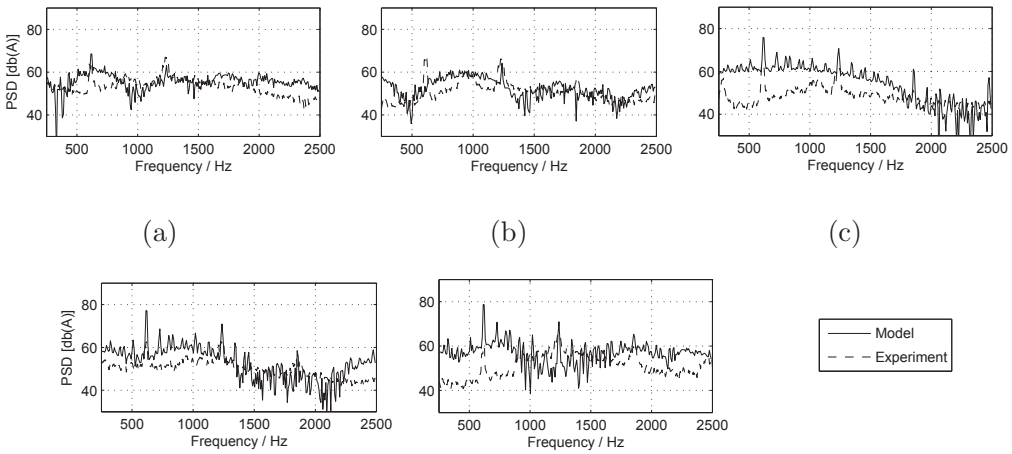

Fig. 20. Power spectral density of a patterned tyre rolling on a ISO-10844 specification road surface at 80 km/hr. An A-weighting has been applied to both the predictions and experimental data. (a) Microphone position 1; (b) Microphone position 2; (c) Microphone position 3; (d) Microphone position 4; (e) Microphone position 5.

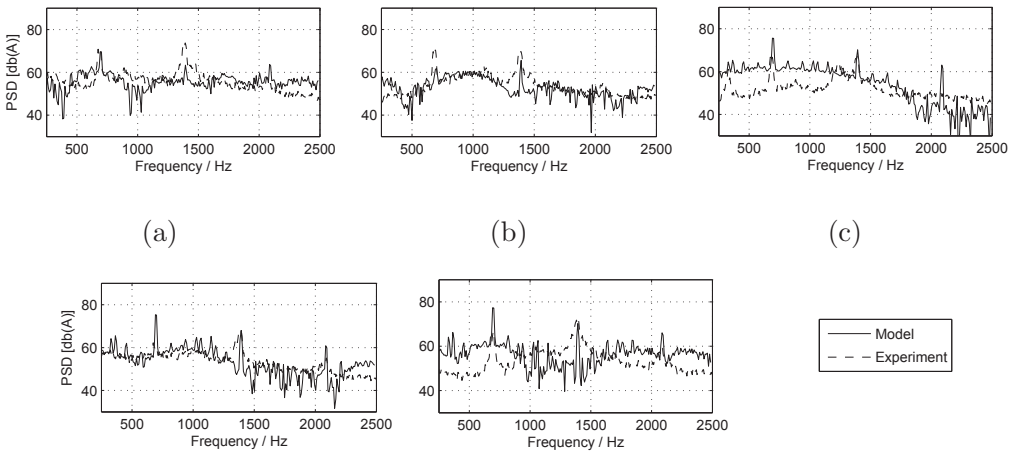

Fig. 21. Power spectral density of a patterned tyre rolling on a ISO-10844 specification road surface at 90 km/hr. An A-weighting has been applied to both the predictions and experimental data. (a) Microphone position 1; (b) Microphone position 2; (c) Microphone position 3; (d) Microphone position 4; (e) Microphone position 5.

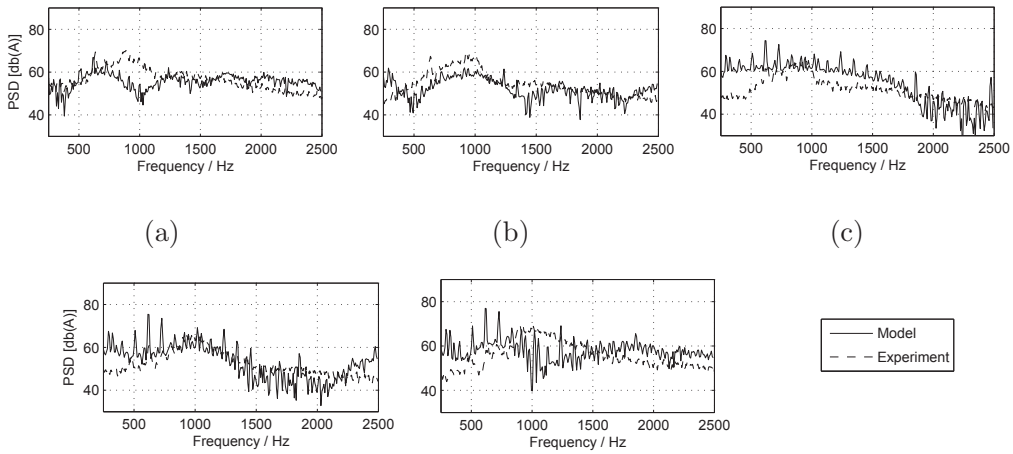

Fig. 22. Power spectral density of a patterned tyre rolling on a hot rolled asphalt road surface at 80 km/hr. An A-weighting has been applied to both the predictions and experimental data. (a) Microphone position 1; (b) Microphone position 2; (c) Microphone position 3; (d) Microphone position 4; (e) Microphone position 5.

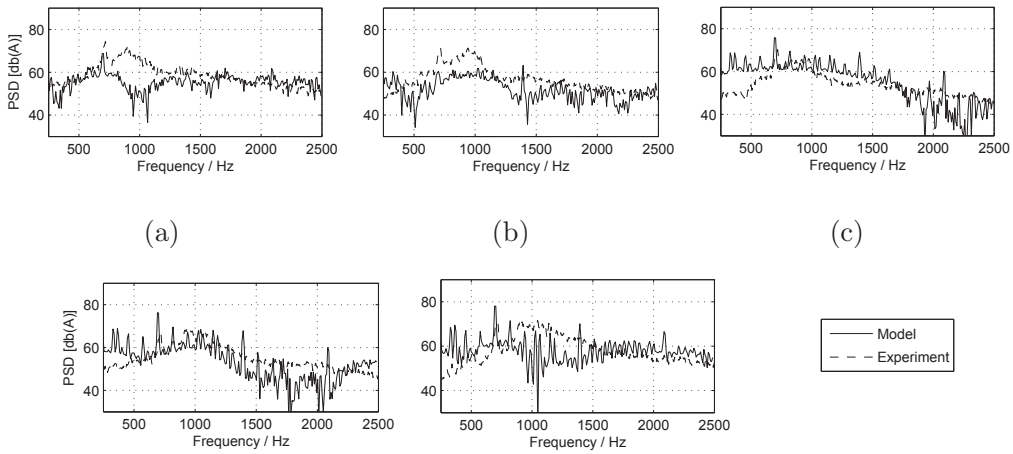

Fig. 23. Power spectral density of a patterned tyre rolling on a hot rolled asphalt road surface at 90 km/hr. An A-weighting has been applied to both the predictions and experimental data. (a) Microphone position 1; (b) Microphone position 2; (c) Microphone position 3; (d) Microphone position 4; (e) Microphone position 5.